Progress In Electromagnetics Research, PIER 69, 267–285, 2007

EFFICIENT NEAR-FIELD COMPUTATION FOR RADIATION AND SCATTERING FROM CONDUCTING SURFACES OF ARBITRARY SHAPE

K. F. A. Hussein

Microwave Engineering Department
Electronics Research Institute
Dokki, Cairo, Egypt

Abstract—A new algorithm for numerical evaluation of the fields in the near zone of conducting scatterers or antennas of arbitrary shape is developed in the present work. This algorithm is simple, fast, robust and is based on a preceding calculation of the current flowing on the conducting surface using the electric filed integral equation (EFIE) technique that employs the Rao-Wilton-Glisson (RWG) basis functions. To examine the validity of the near field computational algorithm developed in the present work, it is applied to calculate the near field due to plane wave incidence on a variety of conducting scatterers. The solution obtained for the fields in the near zone is found to satisfy the boundary conditions on both planar and curved scatterer surfaces and the edge condition for structures possessing edges or corners. The solutions obtained using the new algorithm are compared with those obtained using some commercial packages that employ the finite-difference-time-domain (FDTD). The algorithm defined in the present work gives results which are more accurate in describing the fields near the edges than the results obtained using the FDTD.

1. INTRODUCTION

The integral equation technique is one of the most widely used electromagnetic techniques up till now [1–5]. However, most of the literatures concerned with this technique give attention to the evaluation of the current, input impedance and far field rather than the evaluation of the near field. The present paper concentrates on developing an algorithm that accurately evaluates the near field as a subsequent computation after the evaluation of the current flowing on

the surface of the radiator or scatterer using the EFIE and method of moments (MoM).

The most important and critical quantities to be calculated when treating electromagnetic radiation and scattering problems using computational techniques are the near field and current quantities. The far field can be entirely determined from the current in the scatterer or from the near field in the vicinity of the scatterer. For realizing the validity of the solutions obtained by a numerical technique, the boundary conditions on the scatterer surface and the edge conditions for open scatterers must be satisfied.

An appropriate method that can deal efficiently with the electromagnetic problems of thin conducting surfaces is the EFIE technique, described by Rao, Wilton and Glisson [6]. An integral equation is formulated for the unknown current on the scattering surface. The integral equation is then converted to a linear system of equations, which can be solved using well-known numerical techniques. Once the current distribution on the antenna surface is obtained, the near field, far field and the antenna characteristics can be directly obtained.

The method used in [6] to evaluate the surface integrals required to formulate the EFIE depends on the transformation of the integrands from the Cartesian coordinates to the so-called normalized area coordinates or simplex coordinates. This enables the expression of each integral as a double integral which is evaluated on the area of each triangular patch. For each combination of triangular patch pairs, three independent integrals must be numerically evaluated. The application of such a transformation results in a huge number of double surface integrals which requires a huge computer memory and long computational time.

A more efficient and optimized alternative to compute the integrals computation involved in the EFIE technique when applied to conducting surfaces is used in the present work. This technique depends on dividing each triangular patch into a number of sub-triangles. In this way, the surface integral over each patch is expressed as a finite summation over the sub-triangles constituting this patch. Using the same triangular patches model of the scatterer, the latter technique considerably reduces the numerical effort required for obtaining accurate results for the current on the scatterer.

The geometrical modeling using cubical pieces (as the cells employed in FDTD), is appropriate only for planar or piecewise planar scatterers. For smoothly curved surfaces, cubical pieces are used to build a staircase model, which causes enormous troubles in electromagnetic computations [7]. The staircase model, even if a very

large number of such pieces is used, is still not able to conform the actual surface or boundary. Staircase model possesses corners and edges all over the scatterer model which is not the case for actual smooth surfaces. This results in that some of the near field components may incorrectly exhibit edge behavior at the points of the scatterer surface although the actual surface is smooth. Moreover, the boundary conditions are not accurately satisfied when a staircase model is used. Thus, a staircase model generally results in unavoidable spurious solutions. The analysis of errors introduced by such an approximation has been proposed in the literature for overcoming the problem of staircase model. Some of them are those employing a globally curvilinear grid [8], using contour path FDTD (CPFDTD) [9] and using locally conformal grid [10] for modeling curved surfaces. However, each of the above approaches has its limitations and may suffer from instability. Moreover, much sophistication may be involved in modeling curved surfaces and may be impractical for treating arbitrarily-shaped surfaces. Furthermore, a severe problem may appear when these methods are used to treat closed surfaces; that is for closed structures there is no mechanism for dissipating the spuriously generated energy and, hence, stable meaningful results are not usually obtainable [10].

The most strong point of the EFIE method is its efficient treatment of perfectly or highly conducting surfaces. Only the surface of the scatterer or radiator is meshed; no "air region" around the antenna or the scatterer needs to be meshed. For conducting wire antennas, the treatment is even more efficient since only a one-dimensional discretization of the wire is undertaken. Moreover, the EFIE automatically incorporates the "radiation condition" i.e., the correct behavior of the field far from the source (proportional to $1/r$ in free space). No near-to-far field transformation is required. In the EFIE, the working variable is the current density, from which many important antenna parameters (impedance, gain, radiation pattern etc.) may be derived, some directly and some via straightforward numerical integration. In conclusion, one can state the fact that the EFIE is preferred to FDTD and the other computational techniques for radiation and scattering problems involving perfectly or highly conducting bodies without the existence of inhomogeneous dielectrics or penetrable materials [1]

2. FORMULATION OF THE EFIE FOR THE CURRENT ON THE CONDUCTING SCATTERER

The electric field radiated due to a surface charge density σ and current $\boldsymbol{J}$ flowing on a conducting surface, S, can be obtained by the following

expression.

$$\boldsymbol{E}(\boldsymbol{r}) = -j\omega\boldsymbol{A}(\boldsymbol{r}) - \nabla\Phi(\boldsymbol{r}) \tag{1}$$

where $\boldsymbol{A}(\boldsymbol{r})$ is the magnetic vector potential defined as

$$\boldsymbol{A}(\boldsymbol{r}) = \frac{\mu}{4\pi}\int\limits_S \boldsymbol{J}\frac{e^{-jk|\boldsymbol{r}-\boldsymbol{r}'|}}{|\boldsymbol{r}-\boldsymbol{r}'|}dS', \tag{2}$$

and $\Phi(\boldsymbol{r})$ is the electric scalar potential defined as

$$\Phi(\boldsymbol{r}) = \frac{1}{4\pi\varepsilon}\int\limits_S \sigma\frac{e^{-jk|\boldsymbol{r}-\boldsymbol{r}'|}}{|\boldsymbol{r}-\boldsymbol{r}'|}dS', \tag{3}$$

where $\boldsymbol{r}'$ is a point on S and $\boldsymbol{r}$ is a point in the near or far zone of free space. The surface charge density σ is related to the surface divergence of the current $\boldsymbol{J}$ flowing on S through the equation of continuity,

$$\nabla_s \cdot \boldsymbol{J} = -j\omega\sigma \tag{4}$$

In the following analysis, for simplicity, $\boldsymbol{A}(\boldsymbol{r})$ and $\Phi(\boldsymbol{r})$ are replaced by $\boldsymbol{A}$ and Φ, respectively. Let the conducting surface S be constructed up by Q triangular patches; a pair of them is shown in Fig. 1. Upon this discretization of S, the potentials $\boldsymbol{A}$ and Φ caused by the currents flowing on this surface, can be expressed as follows

$$\boldsymbol{A} = \sum_{n=1}^{N} \boldsymbol{A}_n, \tag{5}$$

$$\Phi = \sum_{n=1}^{N} \Phi_n, \tag{6}$$

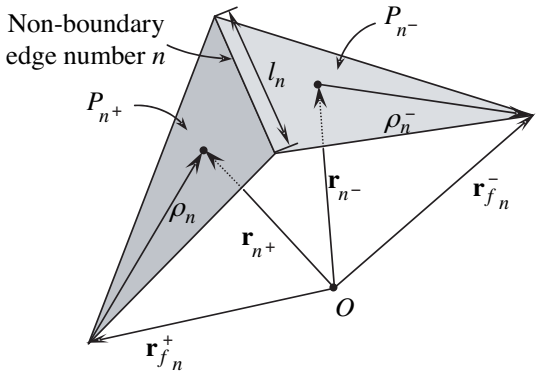

Figure 1. Two triangular patches sharing an edge.

where N is the total number of non-boundary edges of the triangular patches constituting the surface S, $\boldsymbol{A}_n$ and Φ_n are the potentials due to the current component associated with the non-boundary edge number n. These potentials can be decomposed as follows,

$$\boldsymbol{A}_n = \boldsymbol{A}^n_{n^+} + \boldsymbol{A}^n_{n^-}, \tag{7}$$

$$\Phi_n = \Phi^n_{n^+} + \Phi^n_{n^-}, \tag{8}$$

where n^+ and n^- are the numbers of the patches sharing the edge number n; the plus and minus designations denote a positive current reference direction for the non-boundary edge number n; that is, n^+ is the number of the patch of which the current of the non-boundary edge number n is assumed to be flowing out, whereas n^- is the number of the patch into which this current is flowing. Thus $\boldsymbol{A}^n_q$ and Φ^n_q are the potentials due to the part of the current component associated with the non-boundary edge number n and flowing through the patch P_q.

In [6], the current basis function associated with the non-boundary edge number n, is defined as

$$\boldsymbol{f}_n(\boldsymbol{r}') = \begin{cases} \frac{l_n}{2S_{n^+}}\left(\boldsymbol{r}' - \boldsymbol{r}^+_{f_n}\right), & \boldsymbol{r}' \in P_{n^+} \\ \frac{l_n}{2S_{n^-}}\left(\boldsymbol{r}^-_{f_n} - \boldsymbol{r}'\right), & \boldsymbol{r}' \in P_{n^-} \\ 0 & \text{otherwise} \end{cases} \tag{9}$$

where l_n is the length of the shared edge number n, S_{n^+} and S_{n^-} are the areas of the triangular patches P_{n^+} and P_{n^-}, respectively, and $\boldsymbol{r}^{\pm}_{f_n}$ is the vertex of the triangular patch $P_{n^\pm}$, which does not belong to the non-boundary edge number n.

Using the basis function $\boldsymbol{f}_n(\boldsymbol{r}')$, the current $\boldsymbol{J}$ flowing on the conducting surface can be approximated as

$$\boldsymbol{J} = \sum_{n=1}^{N} I_n \boldsymbol{f}_n(\boldsymbol{r}') \tag{10}$$

where I_n is unknown coefficient (of $\boldsymbol{f}_n$ in the current expansion series) and is to be determined by the moment method.

3. DEVELOPMENT OF THE NEAR-FIELD COMPUTATIONAL ALGORITHM

Making use of (2), (3), (4) and (10), one gets the following expressions for $\boldsymbol{A}^n_{n^\pm}$ and $\Phi^n_{n^\pm}$, respectively,

$$\boldsymbol{A}^n_{n^\pm} = \frac{\mu I_n}{4\pi} \int\limits_{P_{n^\pm}} \boldsymbol{f}_n(\boldsymbol{r}') F dS', \tag{11}$$

$$\Phi^n_{n^\pm} = -\frac{\mu I_n}{4\pi j\omega\varepsilon}\int\limits_{P_{n^\pm}} \nabla_s \cdot \boldsymbol{f}_n(\boldsymbol{r}')FdS', \tag{12}$$

where

$$F = \frac{e^{-jkR}}{R}, \tag{13}$$

$$R = |\boldsymbol{r} - \boldsymbol{r}'| \tag{14}$$

Using the definition of $\boldsymbol{f}_n$, given by (9), one gets the following expressions for $\boldsymbol{A}^n_{n^\pm}$ and $\Phi^n_{n^\pm}$, respectively,

$$\boldsymbol{A}^n_{n^\pm} = \pm\frac{\mu I_n l_n}{8\pi S_{n^\pm}}\int\limits_{P_{n^\pm}} \left(\boldsymbol{r}' - \boldsymbol{r}^\pm_{f_n}\right)FdS', \tag{15}$$

$$\Phi^n_{n^\pm} = \mp\frac{I_n l_n}{4\pi j\omega\varepsilon S_{n^\pm}}\int\limits_{P_{n^\pm}} FdS', \tag{16}$$

Dividing each triangular patch into a number of identical sub-triangles as shown in Fig. 2, the integrals in (15) and (16) can be evaluated as follows,

$$\boldsymbol{A}^n_{n^\pm} = \pm\frac{\mu I_n l_n}{8\pi K^2}\sum_{t=0}^{K^2-1}\left(\boldsymbol{r}^t_{c_{n^\pm}} - \boldsymbol{r}^\pm_{f_n}\right)F^t_{c_{n^\pm}}, \tag{17}$$

$$\Phi^n_{n^\pm} = \mp\frac{I_n l_n}{4\pi j\omega\varepsilon K^2}\sum_{t=0}^{K^2-1}F^t_{c_{n^\pm}}, \tag{18}$$

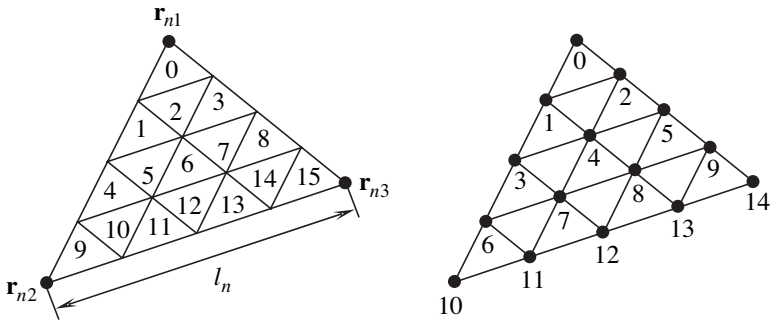

(a) Indices of sub-triangles (b) Indices of vertices of sub-triangles

Figure 2. A triangular-patch divided into a number of identical sub-triangles.

where K is the number of sub-triangles to which a triangular patch is divided, $\boldsymbol{r}_{cq}^{t}$ is the centroid of the sub-triangle number t on the triangular patch P_q,

$$F_{cq}^{t} = \frac{e^{-jkR_{cq}^{t}}}{R_{cq}^{t}}, \tag{19}$$

and

$$R_{cq}^{t} = \left|\boldsymbol{r} - \boldsymbol{r}_{cq}^{t}\right| \tag{20}$$

Let us define the following series,

$$\mathcal{S}_q = \sum_{t=0}^{K^2-1} F_{cq}^{t} \tag{21}$$

$$\boldsymbol{S}_q = \sum_{t=0}^{K^2-1} \boldsymbol{r}_{cq}^{t} F_{cq}^{t} \tag{22}$$

Making use of (21) and (22), expressions (17) and (18) can be rewritten as

$$\boldsymbol{A}_{n^{\pm}}^{n} = \pm\frac{\mu I_n l_n}{8\pi K^2}\left[\boldsymbol{S}_{n^{\pm}} - \mathcal{S}_{n^{\pm}}\boldsymbol{r}_{f_n}^{\pm}\right], \tag{23}$$

$$\Phi_{n^{\pm}}^{n} = \mp\frac{I_n l_n}{4\pi j\omega\varepsilon K^2}\mathcal{S}_{n^{\pm}} \tag{24}$$

The straightforward way of thinking to numerically evaluate the potentials $\boldsymbol{A}$ and Φ suggests that for each non-boundary edge n, the quantities $\boldsymbol{S}_{n^+}, \boldsymbol{S}_{n^-}, \mathcal{S}_{n^+}$, and $\mathcal{S}_{n^-}$ are first calculated using (21), (22) and then the quantities $\boldsymbol{A}_{n^+}^{n}, \boldsymbol{A}_{n^-}^{n}, \Phi_{n^+}^{n}$, and $\Phi_{n^-}^{n}$ are calculated using (23), (24) and finally, the potentials $\boldsymbol{A}$ and Φ are calculated using (5)–(6). However, if this algorithm is applied a considerable time will be wasted because most of the quantities $\boldsymbol{S}_{n^+}, \boldsymbol{S}_{n^-}, \mathcal{S}_{n^+}$, and $\mathcal{S}_{n^-}$ may be calculated two or three times. A more efficient scheme suggests that the quantities $\boldsymbol{S}_q$, $\mathcal{S}_q$ are calculated for $q = 1, 2, 3, \ldots, Q$ and stored in the computer memory. When the expressions (23), (24) are then used, for each n, the proper quantities are restored from the memory. For a closed surface, this method would save two-third the computational time required if the last algorithm were used.

4. CALCULATION OF THE ELECTRIC FIELD IN THE NEAR ZONE

The electric field components can be numerically calculated by discretizing equation (1) in the space as follows.

$$E_x = -j\omega A_x - \frac{\Delta\Phi}{\Delta x} \tag{25}$$

$$E_y = -j\omega A_y - \frac{\Delta\Phi}{\Delta y} \tag{26}$$

$$E_z = -j\omega A_z - \frac{\Delta\Phi}{\Delta z} \tag{27}$$

To enable the above computations, the three-dimensional space is discretized by the 3D main grid shown in Fig. 3 and Fig. 4. For accurate numerical differentiation, the scalar potential Φ is calculated at the points indicated by crosses on the three-dimensional grid shown in Fig. 3 and Fig. 4, whereas the electric field components are calculated

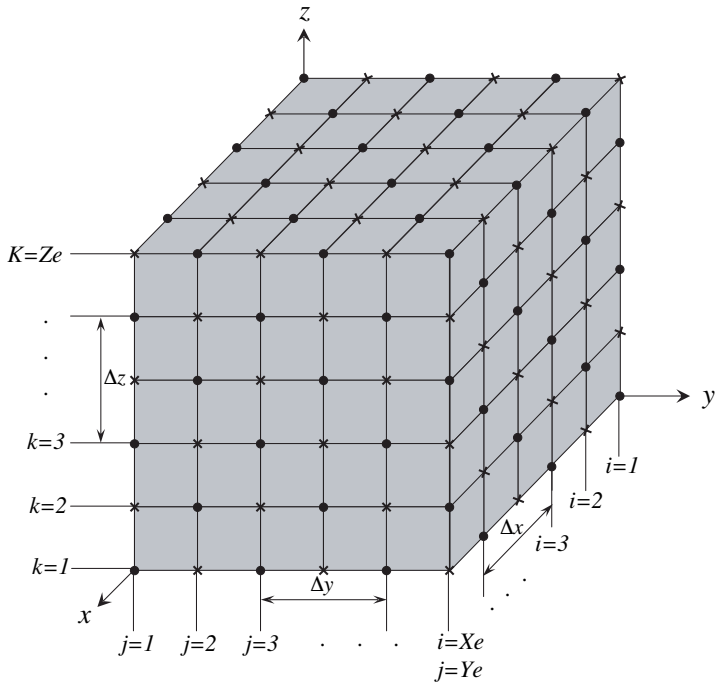

Figure 3. Space discretization to calculate the electric and magnetic fields in the near zone.

at the intermediate points which are indicated by dots. The points of the grid are arranged such that each point is defined by three indices $i = 1, 2, 3, \ldots, I_e$, $j = 1, 2, 3, \ldots, J_e$ and $k = 1, 2, 3, \ldots, K_e$. The selection of the points at which a potential or field quantity is calculated can be described as follows. The scalar potential Φ is calculated at the points whose indices summation $i + j + k$ is even whereas the components of the vector magnetic potential are calculated at the intermediate points, i.e. the points whose indices summation is odd. In this way, the electric field components can be calculated as follows.

$$E_x\Big|_{i,j,k} = -j\omega A_x\Big|_{i,j,k} - \frac{1}{\Delta x}\left(\Phi\Big|_{i+1,j,k} - \Phi\Big|_{i-1,j,k}\right) \tag{28}$$

$$E_y\Big|_{i,j,k} = -j\omega A_y\Big|_{i,j,k} - \frac{1}{\Delta y}\left(\Phi\Big|_{i,j+1,k} - \Phi\Big|_{i,j-1,k}\right) \tag{29}$$

$$E_z\Big|_{i,j,k} = -j\omega A_z\Big|_{i,j,k} - \frac{1}{\Delta z}\left(\Phi\Big|_{i,j,k+1} - \Phi\Big|_{i,j,k-1}\right) \tag{30}$$

It is clear that the components of the electric field are calculated at the same points of calculating the components of the magnetic vector potential. To enable the calculation of all the components of the electric field at all the points of the main grid specified for this, the scalar potential must be calculated at other (auxiliary) points lying just outside the main grid. These auxiliary points are indicated as pentagonal stars as shown in Fig. 4. Table 1 indicates the potential or field component that should be calculated at the points having the designations shown in Fig. 4.

Table 1. The potentials and field components to be calculated at the different points of the main and auxiliary points.

Point symbol	Potentials and field components to be calculated at each point
★	$\boldsymbol{\Phi}$
◈	$\boldsymbol{A_x, A_y, E_x, E_y}$
⊡	$\boldsymbol{A_x, A_z, E_x, E_z}$
■	$\boldsymbol{A_y, A_z, E_y, E_z}$
×	$\boldsymbol{\Phi, H_x, H_y, H_z}$
•	$\boldsymbol{A_x, A_y, A_z, E_x, E_y, E_z}$

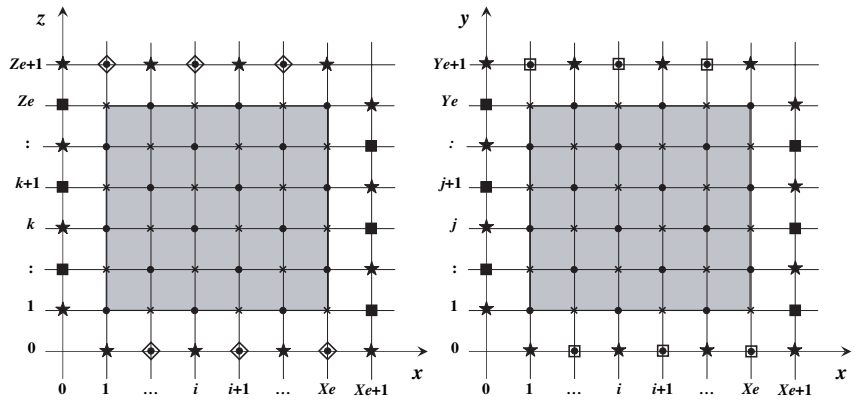

(a) *x*-*z* plane (b) *x*-*y* plane

Figure 4. Auxiliary points are used to calculate the electric field at all the points of the main grid. The shaded area represents the main grid where as the auxiliary points are plotted outside this area.

5. CALCULATION OF THE MAGNETIC FIELD IN THE NEAR ZONE

The magnetic field components can be calculated from the electric field components through the Maxwell curl equation:

$$\mu \frac{\partial \boldsymbol{H}}{\partial t} = \nabla \times \boldsymbol{E} \tag{31}$$

The last equation can be decomposed into three scalar equations and written in the frequency domain as follows.

$$j\omega H_x = \frac{1}{\mu}\left[\frac{\partial E_y}{\partial z} - \frac{\partial E_z}{\partial y}\right] \tag{32}$$

$$j\omega H_y = \frac{1}{\mu}\left[\frac{\partial E_z}{\partial x} - \frac{\partial E_x}{\partial z}\right] \tag{33}$$

$$j\omega H_z = \frac{1}{\mu}\left[\frac{\partial E_x}{\partial y} - \frac{\partial E_y}{\partial x}\right] \tag{34}$$

To numerically calculate the magnetic field components, the last three equations can be discretized in space as follows.

$$H_x = \frac{1}{j\omega\mu}\left[\frac{\Delta E_y}{\Delta z} - \frac{\Delta E_z}{\Delta y}\right] \tag{35}$$

$$H_y = \frac{1}{j\omega\mu}\left[\frac{\Delta E_z}{\Delta x} - \frac{\Delta E_x}{\Delta z}\right] \tag{36}$$

$$H_z = \frac{1}{j\omega\mu}\left[\frac{\Delta E_x}{\Delta y} - \frac{\Delta E_y}{\Delta x}\right] \tag{37}$$

Using the same three-dimensional grid of Fig. 3, the magnetic field components are calculated at the points whose indices summation $i + j + k$ is even, i.e., at the same locations of calculating the scalar potential, Φ; this can be done through the following equations.

$$H_x\Big|_{i,j,k} = \frac{1}{j\omega\mu}\left[\frac{E_y\Big|_{i,j,k+1} - E_y\Big|_{i,j,k-1}}{\Delta z} - \frac{E_z\Big|_{i,j+1,k} - E_z\Big|_{i,j-1,k}}{\Delta y}\right] \tag{38}$$

$$H_y\Big|_{i,j,k} = \frac{1}{j\omega\mu}\left[\frac{E_z\Big|_{i+1,j,k} - E_z\Big|_{i-1,j,k}}{\Delta x} - \frac{E_x\Big|_{i,j,k+1} - E_x\Big|_{i,j,k-1}}{\Delta z}\right] \tag{39}$$

$$H_z\Big|_{i,j,k} = \frac{1}{j\omega\mu}\left[\frac{E_x\Big|_{i,j+1,k} - E_x\Big|_{i,j-1,k}}{\Delta y} - \frac{E_y\Big|_{i+1,j,k} - E_y\Big|_{i-1,j,k}}{\Delta x}\right] \tag{40}$$

The electric field components are calculated at the auxiliary points just outside the main grid, which are indicated as solid square blocks, squares containing dots and rhombuses containing dots as shown in Fig. 4. If this is done, the three components of the magnetic field can be calculated at all the selected points of the main grid, which are indicated by crosses in Figures 3 and 4.

In this way, the six field components $E_x, E_y, E_z, H_x, H_y, H_z$, are all calculated at all the selected points of the main grid.

6. RESULTS AND DISCUSSION

To examine the validity of the near field computational algorithm developed in the present work, it is applied to calculate the near field due to a variety of conducting scatterers. As a first examination, the solution obtained for he fields in the near zone should satisfy the boundary conditions and the edge condition for open structures. The solutions obtained using the present algorithm are, also, compared with those obtained using some commercial packages that employ other computational techniques such as FDTD.

In the following, we present some results concerning the scattering of plane waves from flat square plates and cylindrical structures. For a

stringent test of the employed computational technique, it is intended to include curvatures and/or edges in the scatterer body to examine the boundary conditions and the field behavior at edges.

6.1. Scattering from a Square Plate

A square plate of dimensions $\frac{1}{2}\lambda \times \frac{1}{2}\lambda$ is subjected to a normally incident plane wave polarized such that the electric field is parallel to one of the plate edges. A Cartesian system of coordinates, Fig. 5, is selected such that the plate lies in the xy-plane ($z = 0$) and the electric field is in the x-direction.

The distributions of the total electric field component E_x (incident and scattered) in the planes $z = 0$ and $y = 0$ are presented in gray color scale as shown in Figs. 6a and 6b, respectively. Since the incident electric field is x-directed, the total electric field exhibits the edge behavior at the perpendicular plate edges $x = -0.25\lambda$ and $x = +0.25\lambda$.

To examine the accuracy of proposed algorithm, the same problem is solved using Remcom Inc. "XFDTD" ® package. Fig. 7 presents the electric field distributions in the planes $z = 0$ and $y = 0$ as obtained by this package. The results presented in this Fig. 7 seems to be identical to those presented in Fig. 6.

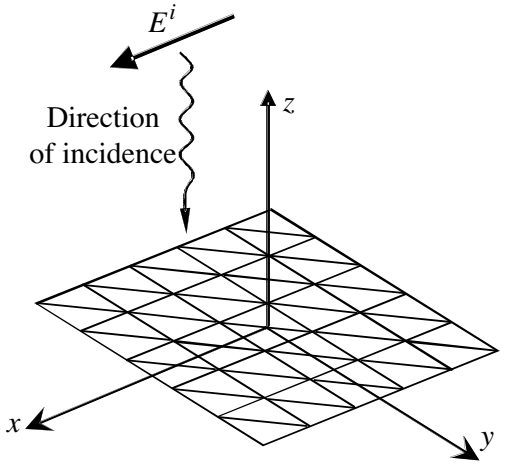

Figure 5. Triangular-patch model of a square plate and direction of incidence and polarization of the plane wave.

For more illustration of the field behavior near the square plate, Fig. 8a shows a plot for the E_x component of the total electric field against x starting from $x = -\lambda$ to $x = +\lambda$. The electric field exhibits singular behavior at the plate edges $x = -0.25\lambda$ and $x = +0.25\lambda$ as

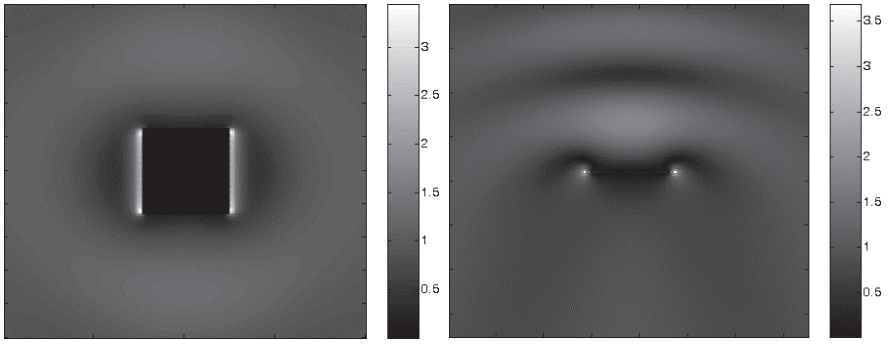

(a) *xy*-plane (b) *xz*-plane

Figure 6. Electric field distribution (E_x) in the near zone due a normally incident plane wave on $0.5\lambda \times 0.5\lambda$ square plate obtained by the computational algorithm proposed in the present work (xy-plane: $z = 0,\ -\lambda < x < \lambda,\ -\lambda < y < \lambda$), ($xz$-plane: $y = 0,\ -\lambda < x < \lambda,\ -\lambda < z < \lambda$).

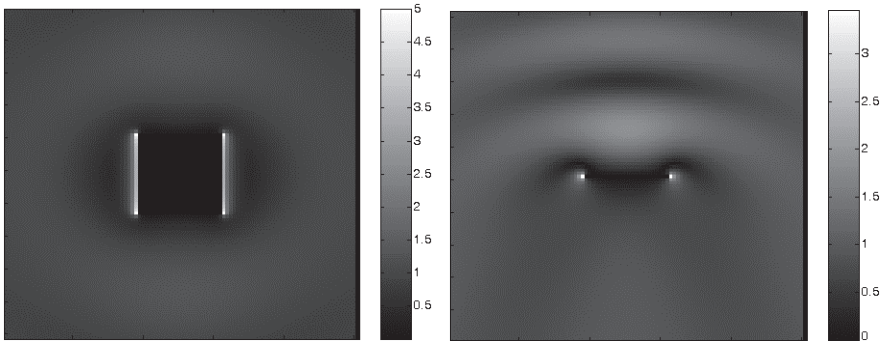

(a) *xy*-plane (b) *xz*-plane

Figure 7. Electric field distribution (E_x) in the near zone due a normally incident plane wave on $0.5\lambda \times 0.5\lambda$ Square plate obtained using Remcom Inc. "XFDTD" ® package (xy-plane: $z = 0,\ -\lambda < x < \lambda,\ -\lambda < y < \lambda$), ($xz$-plane: $y = 0,\ -\lambda < x < \lambda,\ -\lambda < z < \lambda$).

shown in the figure. Despite being of high magnitude at the plate edges, E_x dramatically falls to zero over the range $-0.25\lambda < x < 0.25\lambda$ just to satisfy the boundary condition that yields vanishing the tangential electric field at the plate surface; a behavior which is clear in the figure. On the other hand, Fig. 8b shows a plot for the E_x component of the total electric field against y starting from $y = -\lambda$ to $y = +\lambda$. As shown

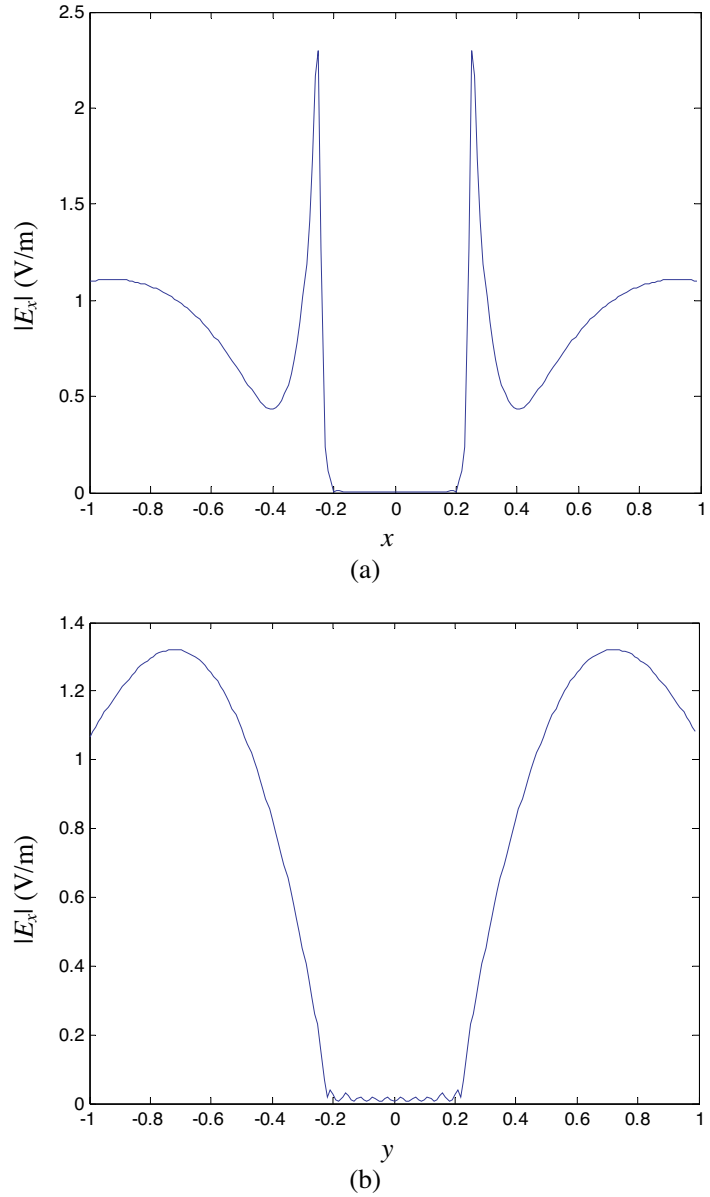

Figure 8. Total electric field (E_x) at the perpendicular and parallel edges of the square plate.

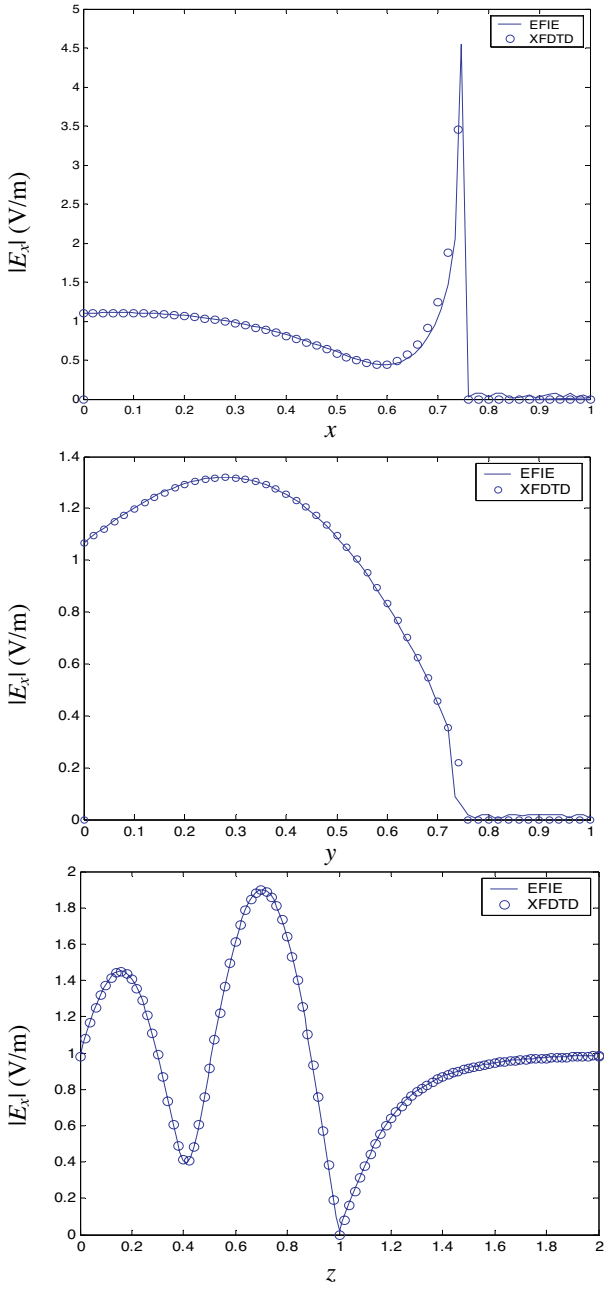

Figure 9. The total electric field (E_x) due to a normally incident plane wave on a $0.5\lambda \times 0.5\lambda$ square plate.

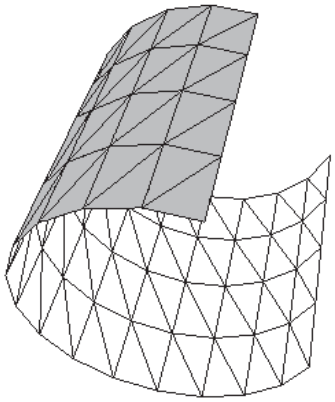

Figure 10. Triangular-patch model of a slotted cylinder of finite length.

in the figure, the electric field satisfies the boundary conditions at the plate surface without exhibiting a singular behavior as it is parallel to the plate edges $y = -0.25\lambda$ and $y = +0.25\lambda$.

Fig. 9 shows a comparison of the behavior of the total electric field (E_x) at the perpendicular and parallel edges of the square plate as obtained in the present work with those obtained by XFDTD. The results obtained by the present work are quite identical to those obtained by Remcom Inc. "XFDTD" ® package, which ensures the validity and accuracy of the applied algorithm.

6.2. Scattering from a Slotted Cylinder

The proposed algorithm is examined here by applying it to get the scattered fields from curved conducting surfaces with edges. A triangular patch model of an axially slotted cylinder of finite length is shown in Fig. 10. It is clear that a small number of triangular patches is enough to accurately model the cylindrical surface.

A cylinder of 0.5λ height, 0.5λ diameter and with an axial slot of width 90° is subjected to a plane wave incident in a direction parallel to its axis and polarized such that the electric field is normal to the plane that contains one of the slot edges and the cylinder axis as shown in Fig. 11.

The distribution of the total angular electric field E_ϕ (incident and scattered) in the plane $z = 0$ is presented in gray color scale as shown in Fig. 12. It is clear the total electric field exhibits the edge behavior at the slot edges $\phi = 0^\circ$ and $\phi = 270^\circ$.

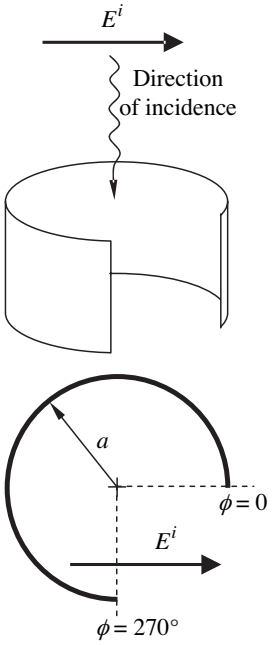

Figure 11. Direction of incidence and polarization of a plane wave incident on a slotted cylinder.

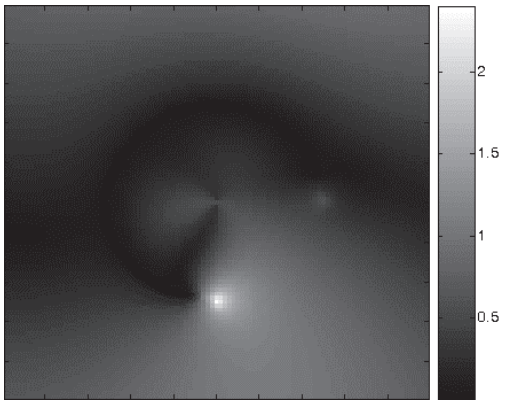

Figure 12. Electric field distribution (E_ϕ) in xy-plane ($z = 0,\ -0.5\lambda < x < 0.5\lambda,\ -0.5\lambda < y < 0.5\lambda$) due to a normally incident plane wave on a slotted cylinder of finite length.

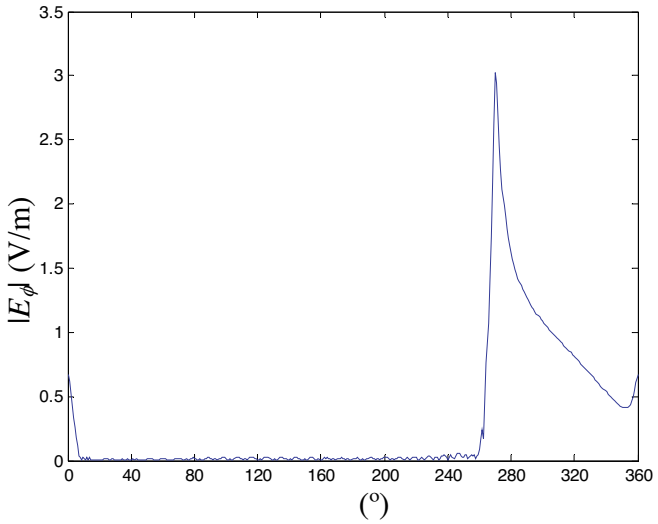

Figure 13. Magnitude of the angular electric field due to a plane wave normally incident on a slotted cylinder of finite length.

For more illustration of the behavior of the near around the slotted cylinder, Fig. 13 shows a plot for the E_ϕ component of the total electric field against ϕ starting from $\phi = 0°$ to $\phi = 360°$. As shown in the figure, the electric field exhibits singular behavior at the slot edges. Despite being of high magnitude at the slot edges, E_ϕ dramatically falls to zero over the range $0° < \phi < 270°$ just to satisfy the boundary condition that yields vanishing the tangential electric field at the cylindrical surface; a behavior which indicates the consistency of the obtained solution.

7. CONCLUSION

A simple, fast and robust algorithm for numerical evaluation of the fields in the near zone for conducting scatterers of arbitrary shape is developed in the present work. The algorithm is built on a preceded calculation of the surface current flowing on the scatterer using the EFIE technique and employing the RWG basis functions. To examine the validity of the near field computational algorithm developed in the present work, it is applied to calculate the near field due to planar and curved conducting scatterers. As a first examination, the solution obtained for he fields in the near zone should satisfy the boundary conditions and the edge condition for open structures. The

solutions obtained using the present algorithm are, also, compared with those obtained using some commercial packages that employ FDTD technique such as Remcom "XFDTD" ®.

REFERENCES

1. Davidson, D. B., *Computational Electromagnetics for RF and Microwave Engineering*, Cambridge University Press, April 2005.
2. Miano, G. and F. Villone, "A surface integral formulation of Maxwell equations for topologically complex conducting domains," *IEEE Trans. Antennas Propagat.*, Vol. 53, No. 12, 4001–4014, Dec. 2005.
3. Yla-Oijala, P., M. Taskinen, and J. Sarvas, "Surface integral equation method for general composite material and dielectric structures with junctions," *Progress In Electromagnetics Research*, PIER 52, 81–108, 2005.
4. Hanninen, I., M. Taskinen, and J. Sarvas, "Singularity subtraction integral formulae for surface integral equations with RWG, rooftop and hybrid basis functions," *Progress In Electromagnetics Research*, PIER 63, 243–278, 2006.
5. Shore, R. A. and A. D. Yaghjian, "A low-order-singularity electric-field integral equation solvable with pulse basis functions and point matching," *Progress In Electromagnetics Research*, PIER 52, 129–151, 2005.
6. Rao, S. M., D. R. Wilton, and A. W. Glisson, "Electromagnetic scattering by surfaces of arbitrary shape," *IEEE Trans. Antennas Propagat.*, Vol. 30, 409–418, May 1982.
7. Cangellaris, A. C. and D. B. Wright, "Analysis of the numerical error caused by the stair-stepped approximation of a conducting boundary in FDTD simulations of electromagnetic phenomena," *IEEE Trans. Antennas Propagat.*, Vol. 39, 1518–1525, Oct. 1991.
8. Lee, J. F., R. R. Panlandech, and R. Mittra, "Modeling three-dimensional discontinuities in waveguides using non-orthogonal FDTD algorithm," *IEEE Trans. Microwave Theory Tech.*, Vol. 40, 346–352, Feb. 1992.
9. Jurgens, T. G. and A. Taflove, "Three-dimensional contour FDTD modeling of scattering from single and multiple bodies," *IEEE Trans. Antennas Propagat.*, Vol. 41, 1703–1708, Dec. 1993.
10. Dey, S. and R. Mittra, "A modified locally conformal finite difference time-domain algorithm for modeling three-dimensional perfectly conducting bodies," *Microwave Optical Tech. Lett.*, Vol. 17, No. 6, 349–352, April 20, 1998.